MASTER'S DEGREE IN NANOSCIENCE, MATERIALS AND PROCESSES

UNIVERSITAT ROVIRA i VIRGILI

Novel carbonized mesoporous silicon biosensor for electrochemical pathogen detection

Marina Bujaldón Velasco

Supervised by Beatriz Prieto Simón

Tarragona, September 2021

Abstract –

Infectious diseases are of great concern at global health level. Therefore, it is of vital importance to develop tools able to identify the pathogen causing the infection, aiming to make sound decisions on the use of antibiotics. Electrochemical biosensors can provide such information. Porous silicon (pSi) has become an interesting material as biosensing platform. In the present work, we propose a novel PFA (polyfurfuryl alcohol)-modified pSi biosensor for the detection of bacterial 16SrRNA. In order to reach such purpose, pSi carbonization, functionalization methods, as well as DNA immobilization, with the corresponding physicochemical characterizations and stability studies were assessed and optimized. Electrografting of 4-aminobenzoic hydrazide (4-ABH) provided the most stable sensing platform for the subsequent immobilization of DNA capture probe among the three functionalization protocols tested: electrografting of 4-aminobenzoic acid (4-ABA) and 4-ABH, and silanization using 3-(aminopropyl)triethoxysilane (APTES). FTIR spectra and electrochemical characterization confirmed successful pSi DNA covalent binding. Next, the sensor electrodes were incubated with various target DNA concentrations and electrochemical measurements were performed. The developed DNA sensors measured the nanochannel blockage resulting from the hindered diffusion of the redox indicator ions added to the measuring solution, occurring after target hybridization. This blockage was measured as an increase of the charge-transfer resistance, indicating that the hybridization between the capture probe and the target DNA successfully occurred. We have successfully developed a pSi-based electrochemical biosensor able to sensitively and selectively detect a target DNA, which is a first step towards the detection of bacterial pathogens through their specific 16SrRNA growth markers.

Keywords – Porous silicon, electrochemical biosensor, polyfurfuryl alcohol, bacterial 16S rRNA detection

I. INTRODUCTION

Microorganisms are extremely important since they play a role in life, the environment, and human bodies. However, certain microorganisms behave as pathogens because they can cause different types of diseases. In such situation, it is fundamental to develop techniques able to detect pathogens.

Staphylococcus aureus (S.aureus) is one of the leading causes of community and hospital-acquired infections which can lead to serious consequences. This human pathogen can cause severe infections but what is more remarkable is its ability to develop antimicrobial resistance[1]. Methicillin-resistant *S. aureus* is the most frequently isolated antibiotic-resistant pathogen in Western countries. It is increasingly showing resistance to multiple antimicrobial agents[2,3]. It is of vital importance to develop tools able to identify the pathogen causing the infection and then assess its antibiotic sensitivity, aiming to make sound decisions on the use of antibiotics. The possibility to obtain accurate information about the pathogen causing the infection at the point of testing in a shorter time is seen as of supreme importance to make quick treatment decisions. Biosensors are analytical devices able to provide such information.

Biosensors represent a rapid and cost-effective strategy for pathogen detection which can be done at the point of testing without the intervention of a specialist user. Moreover, it allows for a faster and more efficient medical intervention. Therefore, these devices can be useful to prevent full-blown infection as well as reducing the spread of the infection[4,5].

Biosensors can be classified according to either their biorecognition element, or the type of transduction[6]. Regarding transduction, there are mainly optical, electrochemical and piezoelectric biosensors[7]. Electrochemical biosensors require more than one electrode, depending on the electrochemical technique (either reference and working electrodes) or reference, counter and working electrodes). The working electrodes can be made of various materials, gold and carbon being the most common ones[8]. Moreover, such electrodes can be commercially available as screen-printed electrodes (SPE). SPE are widely used in bacteria detection[9,10].

Considerable research is being conducted involving porous silicon (pSi) as biosensing platforms[11–14]. It has become an interesting material because of its large diversity of sensor applications. This is due to its several properties: large internal surface area (>100m^2/cm^2), ease of surface functionalization, tuneable pore diameters (from a few nm to several μm), film thickness (from a few nm to the silicon wafer thickness) and refractive index (from 1,1 to 3,3)[15,16].

PSi fabrication via electrochemical anodization is advantageous since the pSi pore size and thickness can be widely and simply varied by selecting the proper electrolyte, current density, current time and concentration of etching solutions[17,18]. Of particular interest for biosensing purposes is the versatile surface chemistry of pSi, that allows a wide range of functionalization mechanisms (e.g hydrosilylation, silanization[19,20], electrografting[21]) to attach functional groups further used to covalently immobilize diverse biomolecules as bioreceptors.

PSi has been successfully applied to the development of optical and electrical sensors[22,23]. However, pSi electrochemical

biosensors have not received as much attention as optical and electrical ones. PSi electrochemical biosensors present several interesting features including high sensitivity, low cost, relatively simple instrumentation, easy miniaturization and portability[24–26]. The combination of electrochemical biosensing approaches and pSi provides an interesting approach to design novel sensing platforms for a wide variety of applications.

Even though the advantageous properties of pSi aforementioned as electrochemical biosensor, one of the main challenges faced is the chemical instability of freshly etched pSi. Highly reactive silicon hydride species present can easily be oxidized resulting in the formation of an insulating SiO_2 layer[27,28]. This limitation makes pSi unsuitable for biosensors with expected long-term stability since aqueous medium is inevitable in most biosensing applications. Several methods have been reported to stabilize freshly etched pSi. Thermal oxidation and carbonization are the most common ones introducing either a silica or carbon coating, respectively, that prevents the degradation of the pSi surface. Guo et al.[25] studied the electrochemical properties of carbon-stabilized pSi: thermally hydrocarbonized pSi (THCpSi) and thermally carbonized pSi (TCpSi). The results of this study enable correlations between the chemical composition of the carbon layer formed onto the pSi nanostructures and the electrochemical behaviour that relates the fast electron transfer kinetics and effective surface area of carbon-stabilized pSi.

As aforementioned, carbon directly bonded to silicon yields a very stable surface species. In such situation, it is required to develop a functionalized carbon-stabilized pSi. Polyfurfuryl alcohol (PFA) is a thermally cross-linked polymer, which is produced via acid-catalysed polymerization of furfuryl alcohol (FA) (Equation 1.1[29]). FA is directly obtainable from the reduction of furfural, which is a renewable chemical produced from agricultural and forestry wastes[30]. Therefore, PFA has been very attractive as a precursor choice for the design of nanostructured carbon materials and carbon-based nanocomposites for several applications such as molecular sieve

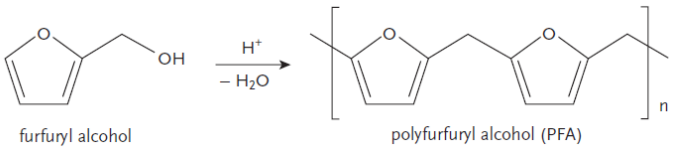

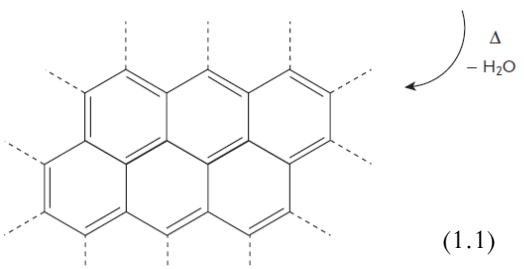

(1.1)

adsorbents and electrodes[31,32]. This will generate high surface-area carbons by polymerization and this reaction will also work inside the pores of the pSi template.

In the present work, we propose to develop a novel PFA-modified pSi biosensor for further detection of bacterial 16SrRNA. The present platform will consist in the polymerization of PFA on pSi followed by its carbonization reaction to get a carbon stabilized pSi device, that features a conductive layer and thus can be used as electrochemical transducer. 16SrRNA from bacteria will be followed by its hybridization to the complementary ssDNA probes immobilized in the pSi layer, taking advantage of the DNA-base pairing interaction. Such hybridization will be electrochemically measured, mainly driven in this case by the increase in the total negative charge upon hybridization, taking advantage of the pore blockage sensing mechanism these porous materials enable. 16SrRNA is a bacterial growth marker[33,34] and thus samples exposed to various antibiotic conditions can be measured to track changes in bacterial growth, indicating bacterial susceptibility to those antibiotics.

In order to reach with such purpose, pSi carbonization, functionalization methods, as well as DNA immobilization, with the corresponding physicochemical characterizations and stability studies need to be optimized.

II. MATERIALS AND METHODS

Fabrication of pSi substrates. PSi was fabricated from p-type silicon wafers with 0.0005 Ω·cm resistivity, and ⟨100⟩-oriented conditions propagating primarily in this direction. Fabrication was performed via electrochemical etching by anodizing the silicon substrates in two steps. Anodization needs two electrodes to maintain charge neutrality and to complete the electrical circuit. A platinum electrode (cathode) supplies electrons to the etching solution, and the silicon wafer (anode) removes electrons from the solution. The etching solution consisted of hydrofluoric acid (HF) as an etchant and ethanol as a surfactant or wetting agent, which lowers the surface tension of the etching solution and helps HF to access the surface.

First, the sample was electropolished with a current density of 350 mA for 30 s in a 3:1 (v/v) solution of aqueous HF (48%) and ethanol, to etch the sacrificial layer. The sacrificial layer was dissolved by replacing the electrolyte with an aqueous solution of NaOH (2 M) for a few min, and the clean wafer was then rinsed with ethanol. The second anodization was performed under a current density of 72 mA for 100 s using a 1:1 (v/v) solution of aqueous HF (48%) and ethanol. Passing electric current through the silicon wafer led to dissolution of silicon atoms and removal

of surface roughness when a critical current density was exceeded. As the wafer was soaked in HF, uniform porosity and thickness of the silicon surface were achieved.

The freshly etched pSi wafers were then modified with PFA by spin coating. In this step, two angular velocity conditions were applied. First, spin coating was done at 700 rpm for 2 min to infiltrate the PFA into the porous structure. Next, the spinning was increased to 1000 rpm for 1 min. Subsequently, to generate the carbon infiltrated pSi composites, the PFA coated pSi was placed into a quartz tube under N_2 flow. First, the temperature was increased 5ºC/min until reaching a temperature of 100ºC. This temperature was maintained for 2 h, and then increased 15ºC/min up to 700ºC. In this time, the temperature was constant for 2 h and 20 min. Finally, the tube cooled back to room temperature under N_2 flow.

PSi surface modification. *Electrografting with 4-aminobenzoic hydrazide:* Hydrazide groups were introduced on pSi by electrografting a diazonium salt generated from 4-aminobenzoic hydrazide (4-ABH). For the solution, it was required 5 mM of $NaNO_2$ in water with 10 mM of 4-ABH in HCl, which were left to react for 30 min in ice, prior to the electrografting process. The electrochemical reductive modification of the pSi was conducted by cyclic voltammetry by scanning the potential between -0.6 and 0.6 V at 100 mV/s and by optimizing the number of scans to 20. Subsequently, the pSi electrodes were rinsed with 0,01 M phosphate-buffered saline (PBS) (pH 7,4) and then subjected to potential scanning between −0.2 and 0.6 V for 10 cycles at 100 mV/s to remove the physisorbed compounds.

The hydrazide-modified surface was immersed in a freshly prepared solution of 2,5% glutaraldehyde in 0,01 M PBS for 1 h to allow further immobilization of the amine-modified DNA capture probe.

Electrografting with 4-aminobenzoic acid: Similar to 4-ABH modification, 4-aminobenzoic acid (4-ABA) was used to introduce carboxyl groups onto the pSi surface. To this purpose, the protocol requires first the generation *in situ* of the corresponding diazonium cations, by mixing 0,2 mM of 4-ABA $NaNO_2$ sodium nitrite (10 mM) prepared in HCl for 30 min in ice before the electrografting step. Electrografting was performed via cyclic voltammetry, scanning the potential from -0,8 V to 0,6 V at a scan rate of 100 mV/s for 6 scans, and further cleaning of the electrode was performed in 0,01 M PBS by scanning the potential from -0,2 V to 0,6 V for 20 cycles. The carboxylic groups of 4-ABA were activated with a 52 mM solution of 1-ethyl-3-(3-dimethylaminopropyl)carbodiimide (EDC) (prepared in a 0,01 M of PBS) for 1 h prior to covalent immobilization of the amine-modified DNA capture probe.

Silanization with 3-(aminopropyl)triethoxysilane. Samples were functionalized in an inert atmosphere of N_2 and room temperature adding 2% (v/v) 3-(aminopropyl)triethoxysilane (APTES) in toluene for 1 h. After thorough rinsing with toluene, ethanol, and acetone and drying under a N_2 stream, the amine-modified surface was immersed in a freshly prepared solution of 100 mg of succinic acid in 4,7 mL of dimethyl sulfoxide (DMSO) and 300 µL of 0,1 M $NaHCO_3$ (pH 9.4) for 30 min. Next, to activate the carboxylic groups, a 52 mM solution of EDC was prepared and added to the samples for 1 h to allow the covalent binding of the amine-modified DNA capture probe.

The aforementioned functionalization protocols were required to covalently link to the pSi the amine-modified ssDNA (5'-NH_2-AGT TAT CCC AGT CTT ATA GGT AGG T-3') capture probe complementary to a 16S rRNA growth factor from *S.aureus* (5'-ACC UAC CUA UAA GAC UGG GAU AAC U-3'). The concentration used for the DNA capture probe incubation was 0,5 µM in 0,01 M PBS. 0,1 M of ethanolamine in 0,01 M PBS was used as blocking agent to deactivate any remaining active groups before any other biomolecules were incubated. As control pSi electrodes, an amine-modified ssDNA capture probe with the following random sequence was used following the same conditions detailed above (5'-NH_2-GTC CAC GCC GTA AAC GAT GTC GAC TTG G-3').

DNA sensing. The DNA target solutions (5'-ACC TAC CTA TAA GAC TGG GAT AAC T-3', DNA sequence equivalent to the 16SrRNA from *S.aureus*) were prepared in 10 mM Tris buffer with 75 mM NaCl (pH 7,4) by using different target ssDNA concentrations: 0,1 pM, 10 pM, 100 pM and 1000 pM.

Target ssDNA were incubated on the pSi samples for 30 min. In the sensing step, electrochemical impedance spectroscopy (EIS) was used as the electrochemical detection technique to quantify the partial nanochannel blockage caused upon DNA binding. EIS measurements were performed prior and after target incubation, to further normalize the data results for the sensing analysis.

Characterization of pSi. Specific properties of the fabricated mesoporous silicon samples were characterized by Field-Emission Scanning Electron Microscopy (FESEM). FESEM (Scios 2 from FEI Company) was used to confirm both pore size and thickness of the samples.

Furthermore, FTIR was also evaluated at each step of functionalization to confirm the different chemical functional groups introduced after carbonization, functionalization and

DNA immobilization. IR spectra were recorded on a Jasco FTIR-4000 series. All spectra were recorded at an average of 64 scans within a range of 400 to 4000 cm^{-1}. The spectra were then analysed using Origin software.

Electrochemical detection protocol. After each step for further sensing, it was required to study the stability of the pSi samples and to monitor any change occurred. Electrochemical measurements were performed on an electrochemical analyser. EIS and Differential Pulse Voltammetry (DPV) were used in the previous mentioned steps, by performing measurements in the presence of the redox species ferrocyanide and ferricyanide, 2 mM each in 0,01 M PBS buffer. Consecutive measurements were carried out until the samples got stabilized. The working electrode area was delimited to 7.5 mm diameter by an O- ring. An Ag/AgCl (3 M NaCl) electrode and a platinum wire were used as reference and counter electrodes, respectively placed into a Faraday cage. DPV measurements were performed within a potential range of -0,18 to 0,6 V. EIS measurements were performed under open circuit potential conditions at 0,2 V, with a frequency range from 0,1 to 10000 Hz. All the data were analyzed using Origin and IviumSoft software. Both EIS and DPV were used to measure the stability of the samples for each pSi surface modification. Apart from being an excellent characterization technique, faradaic EIS was used to directly detect the DNA hybridization between the capture probe and the target DNA.

III. RESULTS AND DISCUSSION

PSi pore size and thickness. Since pSi pore size and thickness are important for DNA electrochemical detection based on pore blockage, FE-SEM images of the samples were taken to assess the effect of the applied current, time and HF concentration on the electrochemical etching, and the PFA concentration and spinning conditions on the carbonization step. In these samples, based on an applied current of 72 mA, and after performing the carbonization step, pore diameter sizes with an average of 23±2 nm were formed, as observed in Figure 1A. Given that each nucleotide is approximately 0,3 nm and the length of the used DNA sequence is, therefore, 7,5 nm, pore sizes of the pSi surface was set to approximately 20 nm for efficient detection, as it has been previously demonstrated[35]. As observed in **Figure 1A**, some pores were distributed non-uniformly. This can be due to the damage between the pore walls causing the formation of larger cavities[36].

PSi thickness could be controlled by applying the same current and by varying the time[37,38]. Images were taken from the cross-section to study the thickness of the samples (**Figure 1B**). As observed, and by applying the same current for 100 s, thickness average was 2,27 µm.

Optimization of pSi carbonization. Optimization of the pSi carbonization process was one of the main steps before any other reaction occurred. This step is crucial because getting carbonized samples will provide them with conductivity, enabling their use for electrochemical measurements. We wanted to explore a new carbon-stabilized platform (comparing the previous study aforementioned with THC and TC devices[25]) to widen the choice, to avoid carbonization in the presence of acetylene (with the risks involved) and to get a platform stable in a wider range of potential (both THC and TC are limited to potentials higher than -0,4 or 0,3 V up to potentials lower than 0,8 or 0,9 V).

The carbonization via PFA procedure (up to 700ºC under flowing N_2 for 5 h) yields a carbon-stabilized pSi matrix. The morphology of these materials is maintained upon carbonization even though the pore size average slightly decreases[15,39]. Once the

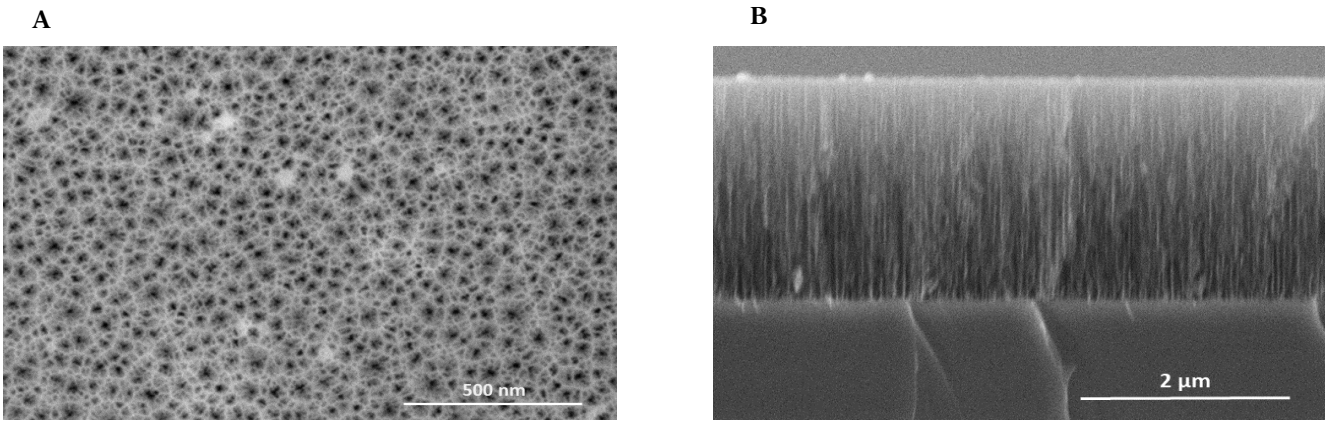

Figure 1. FESEM images A) top view and B) cross section of the PFA-modified pSi layer with two-step electrochemical etching and by applying a current of 72 mA for 100 s

pSi freshly etched samples were coated with PFA by spin coating, the spinning conditions were optimized in order to obtain a final stable platform with the appropriate pore size. Once added the PFA solution on the samples, spin coating at 300 rpm was performed for 1 min and then the speed was increased to 4000 rpm for 2 min. To check the stability of these samples, electrochemical measurements were performed by EIS and DPV.

Even though samples were stable (data not shown), the average pore size was not the suitable one for this study, since pores were not large enough (16±4 nm). Next, spin coating conditions were modified, increasing the speed up to 1000 and 3000 rpm for 2 min and then to 4000 rpm for 1 min to determine the effect on pore size and stability. Moreover, electrochemical measurements were performed along consecutive hours in a day, and along consecutive days to determine the stability of the samples over time. Increasing the spin coating speed up to 1000 rpm for 2 min and then 4000 rpm for 1 min generated larger pores (average pore size of 23±2 nm), compared to the previous spin coating conditions, and samples were stable. However, samples prepared at 3000 rpm spin coating speed were not stable (**Table 1**), since the impedance Rct and current values were not showing similar values (showing increasing and decreasing trends, respectively).

***Table 1**. Stability study of samples prepared at two different spin coating speeds (1000 and 3000 rpm), by comparing the charge-transfer resistance (Rct) and oxidation current (Iox) measured at different times*

		1000 rpm / 4000 rpm	3000 rpm / 4000 rpm
Pore size		23 nm	34 nm
Rct	**1h**	24 Ω	126 Ω
	2h	25 Ω	177 Ω
	3h	27 Ω	236 Ω
	4h	25 Ω	280 Ω
	1 day	25 Ω	373 Ω
Iox	**1h**	158 µA	189 µA
	2h	168 µA	141 µA
	3h	170 µA	98 µA
	4h	168 µA	75 µA
	1 day	162 µA	60 µA

Stability study after surface modification (APTES, 4-ABA and 4-ABH). The reliability of these pSi platforms strongly depends on acquiring a proper immobilization of the capture probe on the samples. This can be achieved through covalent immobilization of such biomolecules[40]. In such situation, three different functionalization protocols have been performed with the goal of getting conclusive results for a stable and reproducible platform.

It was required to work with triplicates for each functionalization for the purpose of studying the reproducibility of all modified samples. PSi samples were electrochemically characterized using EIS and DPV to monitor the stability by analysing the data for all measurements. The EIS technique is very sensitive to the inner surface of porous materials and allows to gather easily additional information on the modified surface of pSi[41]. In order to quantitatively interpret EIS responses, the experimental EIS spectra were fitted using the equivalent circuit presented in **Figure 2**. In this model R1 represents the electrolyte resistance, C1 represents the constant phase element (it takes into account any deviation from a real capacitor), W1 is the Warburg impedance and R2 represents the charge-transfer resistance (the resistance associated with electrochemical kinetics).

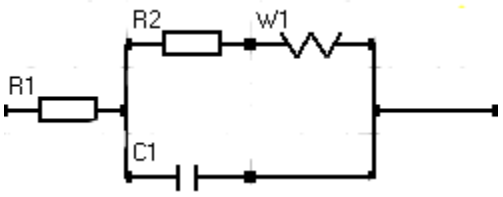

***Figure 2**. Equivalent circuit model for EIS analysis*

For DPV analysis, it was determined the oxidation current of the redox probe added in solution, reflecting the effect of the changes on the pSi surface on its diffusion through the pSi pores.

Nine samples were electrochemically etched and further functionalized for this step. For all samples, at least three consecutive measurements were performed for both electrochemical techniques to confirm the stability of the samples after functionalization. For each type of pSi surface modification, the three samples prepared showed similar results. In this way, one result for APTES, 4-ABA and 4-ABH modification is represented in **Table 2**. Relative standard deviation (RSD) was calculated for each functionalization, by taking the last three measurements for EIS and DPV, and by applying the equation: *RSD= (Standard deviation x 100)/mean*. RSD values inform about the stability of the samples.

As shown in **Table 2**, and having the aid of **Figure S1** from 'Supporting Information', for EIS measurements, the sample

functionalized with APTES was not showing a stable platform. The 25% of RSD, corresponding to a continuous increase of the Rct, could be probably caused by an oxidation of the porous material. DPV for the same sample, showed a decrease in the current oxidation peaks, sustaining the data results from EIS, and indicating that the sample was not stable. Additionally, as **Figure S1B** shows, two current peaks were observed in the three measurements. We can reach to two hypotheses regarding these two peaks. From one side, silanization could have not been homogeneous and thus there are two surfaces, one silanized that leads to the highest oxidation potential, and another one not silanized that allows the lowest potential. Another hypothesis is that the surface partly degrades over time (the degraded surface being responsible of the highest potential, and the non-degraded one being responsible of the lowest potential).

In the case of the sample functionalized with 4-ABA, and as shown in **Table 2**, the sample was not stable. For EIS, as the number of measurements increased, Rct values were shifted to higher values. DPV also showed a similar trend to that of APTES-modified pSi. The current peaks decreased over time, as the number of measurements increased, leading to an RSD value that confirms the lack of stability.

For 4-ABH modified pSi samples, the results showed a different trend as the two aforementioned functionalizations. In the case of EIS measurements, the Rct values were similar, indicating that the sample was stable. Subsequently, DPV measurements were carried out to confirm the stability and, as observed, the current peaks values showed a similar trend between them. The low RSD values obtained confirmed the stability of the pSi samples functionalized with 4-ABH, indicating that further steps could be performed.

***Table 2**. Stability measurements for APTES, 4-ABA and 4-ABH functionalizations. RSD: relative standard deviation*

	APTES	4-ABA	4-ABH
Rct	36 Ω	96 Ω	1061 Ω
	49 Ω	111 Ω	1059 Ω
	60 Ω	147 Ω	1055 Ω
RSD	25%	22%	0,3%
Iox	665 µA	138 µA	111 µA
	647 µA	129 µA	108 µA
	615 µA	108 µA	111 µA
RSD	4%	12%	2%

FTIR spectra of pSi platform. Once the functionalization protocol providing the most stable pSi platform was identified, the next step was the covalent immobilization of the DNA capture probe on the 4-ABH-modified pSi samples. Upon 4-ABH electrografting onto the PFA-modified pSi substrates, hydrazide groups were available for further DNA immobilization. Samples were then incubated with glutaraldehyde so that the aldehyde group could react with the hydrazide to form hydrazone linkages[42]. Glutaraldehyde was used as a bifunctional linker between the hydrazide-functionalized electrode and the NH_2-terminated DNA probe. The reaction with the NH_2 group on the DNA probe led to an imine bond enabling covalent immobilization of the DNA probe on the pSi electrode surface.

FTIR was used to confirm that all steps were performed correctly. Regarding PFA pSi (**Figure 3A**), it is important to highlight the presence of a broad OH-stretching band near 3400 cm^{-1} [43–45]. Unsaturated carbon double bond stretching at 1600 cm^{-1} and CH_3 symmetric deformation mode of Si–CH_3 at 1250 cm^{-1} appeared. It could also be observed the bending C-H band arising from the aromatic compound around 1650 cm^{-1}[25]. PSi samples also showed characteristic peaks for Si-O-Si bonds from 900 to 1100 cm^{-1} [46]. **Figure 3B** shows the FTIR spectra of pSi 4-ABH modified. A band around 3400 cm^{-1} was due to the characteristic N-H stretching vibration. The presence of C–N groups was confirmed by the band at 1500 cm^{-1}. The carbonyl C=O stretching modes are reported in the region 1650 cm^{-1} [47,48]. For glutaraldehyde FTIR spectra (**Figure 3C**), the broad band at 3400 cm^{-1} shows the presence of O-H stretching[49]. It was also observed a CH_2 stretching at 2900 cm^{-1}. A CHO band from the aldehyde group at 1700 cm^{-1} was also observed[50]. A C=N strong band can be observed at 1400 cm^{-1} that may indicate the hydrazone formation. Finally, the FTIR spectrum of the pSi sample upon covalent immobilization of the DNA capture probe (**Figure 3D**) shows a band around 1650 cm^{-1} that corresponds to the stretching vibration of the C=N group of the imine group. The broad peak at approximately 3400 cm^{-1}, which can be assigned to the N-H stretch of the amine group from the NH_2-modified DNA, suggests that not all amine groups were converted to imine[51]. In any case, the imine peak confirms that DNA was successfully immobilized.

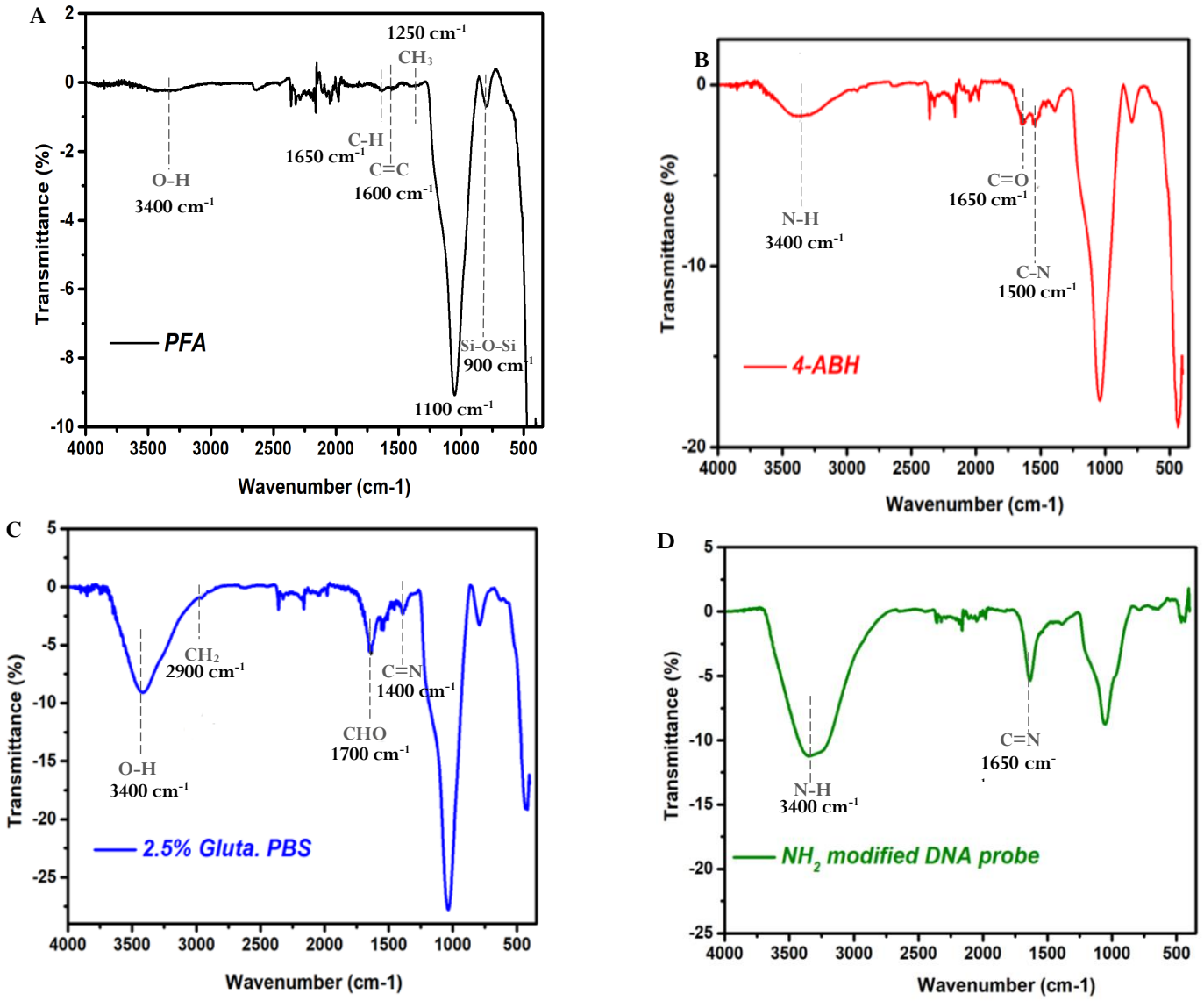

Figure 3. FTIR spectra for A) PFApSi, B) 4-ABH-modified pSi, C) 4-ABH-modified PFApSi after reaction with glutaraldehyde and D) 4-ABH-modified PFApSi with covalently bound DNA capture probe

Electrochemical 4-ABH characterization. To confirm the immobilization of the DNA on the pSi samples prior to the sensing step, EIS measurements were performed prior and after DNA incubation. The results from **Figure 4** show an increase in Rct after the incubation of ssDNA on the pSi sample, from 622 Ω for pSi to 929 Ω for pSi-ssDNA, indicating that the capture probe was immobilized.

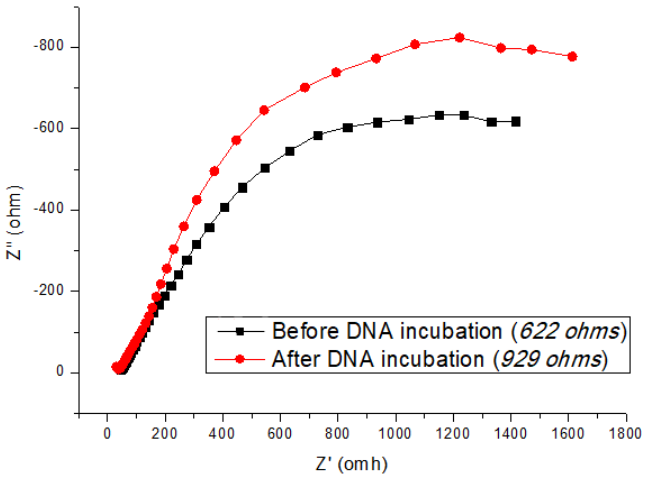

Figure 4. EIS measurements prior and after capture DNA incubation

DNA sensing. To confirm the hybridization between the immobilized capture DNA probe and the target DNA, electrochemical sensing was performed by employing EIS measurements. To that purpose, added to the sensors already prepared, control sensors were prepared by immobilizing a random DNA sequence which was expected to show no affinity for the target DNA. For the sensing step, DNA oligonucleotides corresponding to the *S. aureus* 16SrRNA sequence reported above were incubated both on the sensor and control surfaces. We have worked with DNA instead of RNA due to the fact that is cheaper and much easier to work with DNA than RNA (DNA is less prone to degradation and we do not need to work with RNase-free solutions). Moreover, DNA can work as a good model system, easy to translate later to RNA targets. So, the optimization of the platform and working protocols can be performed working with a DNA target. The last step prior to testing real samples would be the comparison of the performance using DNA and RNA as the analyte.

EIS measurements were performed to confirm hybridization of the target DNA on the sensor surface, while no signal was expected from controls. In Faradaic EIS Rct values are often a good indicator of changes in the electron transfer of a redox indicator, present in solution ($[Fe(CN)_6]^{3-/4-}$), on the electrode surface, which can be the result of surface blocking effects. Here those effects, exerted by the hybridization of the target DNA to the immobilized capture probe, are amplified by the electrostatic repulsion between the redox indicator in solution and the increase in the total negative charge on the surface[52].

Figure 5 shows the calibration curves for three sensors and one control, showing the error bars indicating the variability between sensors, while **Figure 6** shows the Nyquist diagram obtained for one sensor and one control.

These results confirmed that the hybridization events that happened inside the nanochannels caused their partial blockage, hindering the diffusion of $[Fe(CN)_6]^{3-/4-}$. As a result, an increase in Rct was observed due to a combination of steric hindrance and the increased repulsion between the negatively charged DNA (increase in total negative charge upon hybridization) and the negative redox indicator ions[53]. The absence of a significant change in Rct observed for the control sensor (as shown in **Figure 5**) demonstrated the selectivity and sensitivity of the developed DNA sensor for the target DNA.

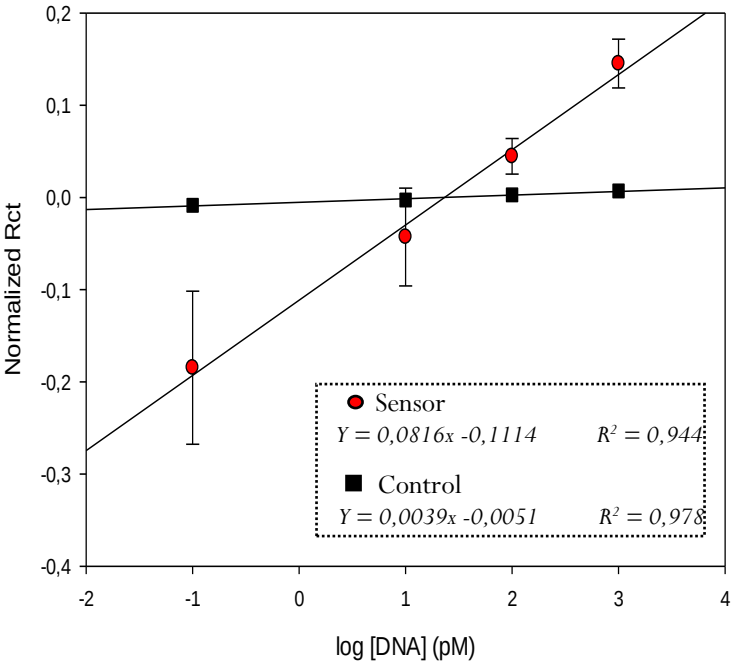

Figure 5. Calibration curves for 3 sensors (red) and one control (black)

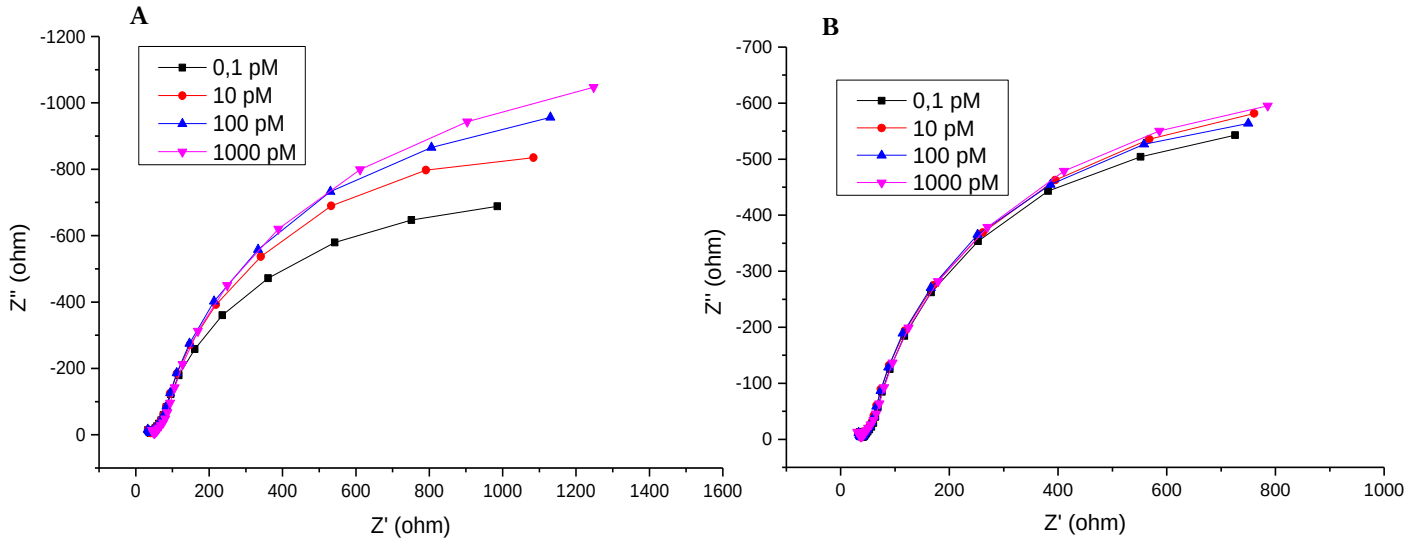

Figure 6. EIS data obtained from A) DNA sensor and B) control sensor, upon incubation of target concentrations from 0,1 to 1000 pM

Even though we could see promising results, this is a preliminary experimentation and some parameters need to be optimized. In the case of pSi carbonization, more analysis research should be done regarding to the pore size and thickness, by playing with the PFA concentration, spin coating and etching conditions. With respect to the results obtained from the three functionalization strategies, other functionalization protocols could be explored, even though the results showed that for 4-ABH, the samples were stable. Regarding working conditions, capture probe concentration, as well as incubation time, should be optimized in order to confirm the results and obtain a reproducible platform.

IV. CONCLUSIONS

We have developed a new electrochemical sensor based on pSi that selectively detects a specific DNA sequence that is of interest. We have worked with a DNA sequence equivalent to the 16SrRNA of *S.aureus*, as a previous step. After completing all the optimization steps, the sensing platform is expected to allow the confirmation of *S.aureus* infection through the detection of such specific bacterial growth biomarker. The present platform consisted on the polymerization of PFA on pSi followed by its carbonization reaction. This provided a conductive layer on pSi to be further used as an electrochemical transducer. We could confirm that carbonization of the pSi led to a stable platform that was required for further surface modifications. 4-ABH-modified PFApSi demonstrated to be the most stable platform, compared to 4-ABA- and APTES-modified platforms, as shown by the RSD values associated to Rct and Iox values obtained from consecutive EIS and DPV measurements, respectively. Moreover, FTIR spectra and electrochemical characterization results demonstrated that the capture DNA probe was successfully immobilized on the pSi platform. In addition, we have demonstrated that by using EIS it is possible to determine modifications in the electrical properties of pSi platforms upon the DNA hybridization reaction. The results indicated that the hybridization between the capture probe and the target DNA occurred with an increase of the Rct. Using a calibration curve, a good correlation between Rct and DNA concentration in the range of 0,1 pM to 1000 pM was demonstrated.

This kind of biosensor can provide ease of miniaturization, high sensitivity, low cost, as well as being a label-free method of detection. Furthermore, the idea is to fabricate a wearable biosensor that enhances clinical surveillance in the patient bacterial infection to help clinicians detect risk so they can intervene earlier and help improve care for patients.

V. ACNOWLEDGMENTS

This project has been carried out with the assistance of the research group Nanoelectronic and Photonic Systems (NEPHOS). I especially want to acknowledge Beatriz Prieto Simón, supervisor of this work, for her guidance, time and dedication. Not least, I also appreciate the support and learning that I received from the people with whom I have had the privilege of sharing laboratory workbench.

VI. REFERENCES

1. Schito, G. C. *Clinical Microbiology and Infection* vol. 12 3–8 (2006).
2. Fontecha Gómez, B. J. & Sánchez Ferrín, P. *Rev. Esp. Geriatr. Gerontol.* **45**, 3–4 (2010).
3. Chen, C. J. & Huang, Y. C. *Clinical Microbiology and Infection* vol. 20 605–623 (2014).
4. Ali, A. A., Altemimi, A. B., Alhelfi, N. & Ibrahim, S. A. *Biosensors* vol. 10 (2020).
5. Ahmed, A., Rushworth, J. V., Hirst, N. A. & Millner, P. A. *Clin. Microbiol. Rev.* **27**, 631–646 (2014).
6. Kaur, H., Bhosale, A. & Shrivastav, S. Biosensors: *Int. J. Heal. Sci. Res.* **8**, 315–333 (2018).
7. Pejcic, B., Marco, R. De & Parkinson, G. *Analyst* **131**, 1079–1090 (2006).
8. Lucarelli, F., Marrazza, G., Turner, A. P. F. & Mascini, M. *Biosens. Bioelectron.* **19**, 515–530 (2004).
9. Vu, Q. K. *et al. Mater. Today Commun.* **26**, (2021).
10. Torre, R., Costa-Rama, E., Nouws, H. P. A. & Delerue-Matos, C. *Biosensors* vol. 10 139 (2020).
11. Jane, A., Dronov, R., Hodges, A. & Voelcker, N. H. *Trends in Biotechnology* vol. 27 230–239 (2009).
12. Fauchet, P. M. in 293–323 (Springer, Boston, MA, 2009).
13. Gupta, B., Zhu, Y., Guan, B., Reece, P. J. & Gooding, J. J. *Analyst* vol. 138 3593–3615 (2013).
14. Ensafi, A. A., Abarghoui, M. M. & Ahmadi, N. in *Handbook of Porous Silicon: Second Edition* vols 2–2 1275–1291 (Springer International Publishing, 2018).
15. Sailor, M. J. in *Porous Silicon in Practice* 189–227 (Wiley-VCH Verlag GmbH & Co. KGaA, 2012).
16. Yang, X. *et al. Fuel Cells* **21**, 52–57 (2021).
17. Rodriguez, G. A., Lawrie, J. L. & Weiss, S. M. in *Porous Silicon for Biomedical Applications* 304–333 (Elsevier Ltd., 2014). doi:10.1533/9780857097156.2.304.
18. Roychaudhuri, C. *Sensors and Actuators, B: Chemical* vol. 210 310–323 (2015).
19. Kim, D. *et al.* Facile Surface *J. Am. Chem. Soc.* **138**, 15106–15109 (2016).
20. Zhang, D. X. *et al. Sci. Rep.* **9**, 1–11 (2019).
21. Clements, L. R. *et al. Phys. Status Solidi Appl. Mater. Sci.* **208**, 1440–1445 (2011).
22. Setzu, S., Monduzzi, M., Mula, G. & Salis, A. in *Biosensors - Emerging Materials and Applications* (InTech, 2011). doi:10.5772/17068.
23. Massad-Ivanir, N. *et al. Sci. Rep.* **6**, 1–12 (2016).
24. Ensafi, A. A., Abarghoui, M. M. & Ahmadi, N. in *Handbook of Porous Silicon: Second Edition* vols 2–2 1275–1291 (Springer

International Publishing, 2018).
25. Guo, K. *et al.* Porous Silicon *Adv. Funct. Mater.* **29**, 1809206 (2019).
26. Roychaudhuri, C. *Sensors and Actuators, B: Chemical* vol. 210 310–323 (2015).
27. Pérez-Ràfols, C. *et al. Electrochim. Acta* **377**, 138077 (2021).
28. Sailor, M. J. in *Handbook of Porous Silicon* 355–380 (Springer International Publishing, 2014).
29. Sailor, M. J. (Wiley-VCH, 2012).
30. Wang, H. & Yao, J. *Industrial and Engineering Chemistry Research* vol. 45 6393–6404 (2006).
31. Burket, C. L., Rajagopalan, R., Marencic, A. P., Dronvajjala, K. & Foley, H. C. *Carbon N. Y.* **44**, 2957–2963 (2006).
32. Pranger, L. A., Nunnery, G. A. & Tannenbaum, R. *Compos. Part B Eng.* **43**, 1139–1146 (2012).
33. Woo, P. C. Y., Lau, S. K. P., Teng, J. L. L., Tse, H. & Yuen, K. Y. Then and now: *Clinical Microbiology and Infection* vol. 14 908–934 (2008).
34. Tran, Q., Pham, D. T. & Phan, V. *BMC Bioinformatics* **18**, 499 (2017).
35. GUO, K.. (2020)
36. Rahimi, F. *et al. Cell J.* **20**, 584 (2019).
37. Husairi, F. S. *et al. AIP Conf. Proc.* **1963**, (2018).
38. Chiang, C.-C. & Lee, B. T.-H. *Sci. Reports 2019 91* **9**, 1–9 (2019).
39. Tsang, C. K., Kelly, T. L., Sailor, M. J. & Li, Y. Y. (2012)
40. Sam, S. *et al. Langmuir* **26**, 809–814 (2010).
41. Mula, G. *et al.* (2014)
42. Hermanson, G. T. *Bioconjugate Tech.* 275–298 (2013)
43. Kim, T., Jeong, J., Rahman, M., Zhu, E. & Mahajan, D. *Korean J. Chem. Eng* **31**, 2124–2129 (2014).
44. Lori, J., Myina, O., Ekanem, E. J. & Lawal, A. O. *undefined* (2011).
45. D'Amico, F. *et al. Spectrochim. Acta Part A Mol. Biomol. Spectrosc.* **262**, 120090 (2021).
46. Zhao, Y., Lawrie, J. L., Beavers, K. R., Laibinis, P. E. & Weiss, S. M. *ACS Appl. Mater. Interfaces* **6**, 13510–13519 (2014).
47. Prieto-Simón, B., Saint, C. & Voelcker, N. H. *Anal. Chem.* **86**, 1422–1429 (2014).
48. V, A., A, J., K, C., S, P. & S, M. *Spectrochim. Acta. A. Mol. Biomol. Spectrosc.* **108**, 100–114 (2013).
49. Ramasubramaniam, S., Govindarajan, C., Nasreen, K. & Sudha, P. N. **21**, 95–109 (2013).
50. Cacho-Bailo, F., Etxeberría-Benavides, M., Karvan, O., Téllez, C. & Coronas, J. (2014)
51. Al-Shuja'a, O. *et al. J. Mater. Sci. Chem. Eng.* **5**, 11–21 (2017).
52. Park, J.-Y. & Park, S.-M. *Sensors (Basel).* **9**, 9513 (2009).
53. Keighley, S. D., Estrela, P., Li, P. & Migliorato, P. *Biosens. Bioelectron.* **24**, 906–911 (2008).

Supporting information

Novel carbonized mesoporous silicon biosensor for electrochemical pathogen detection

Marina Bujaldón Velasco
Supervised by Beatriz Prieto Simón

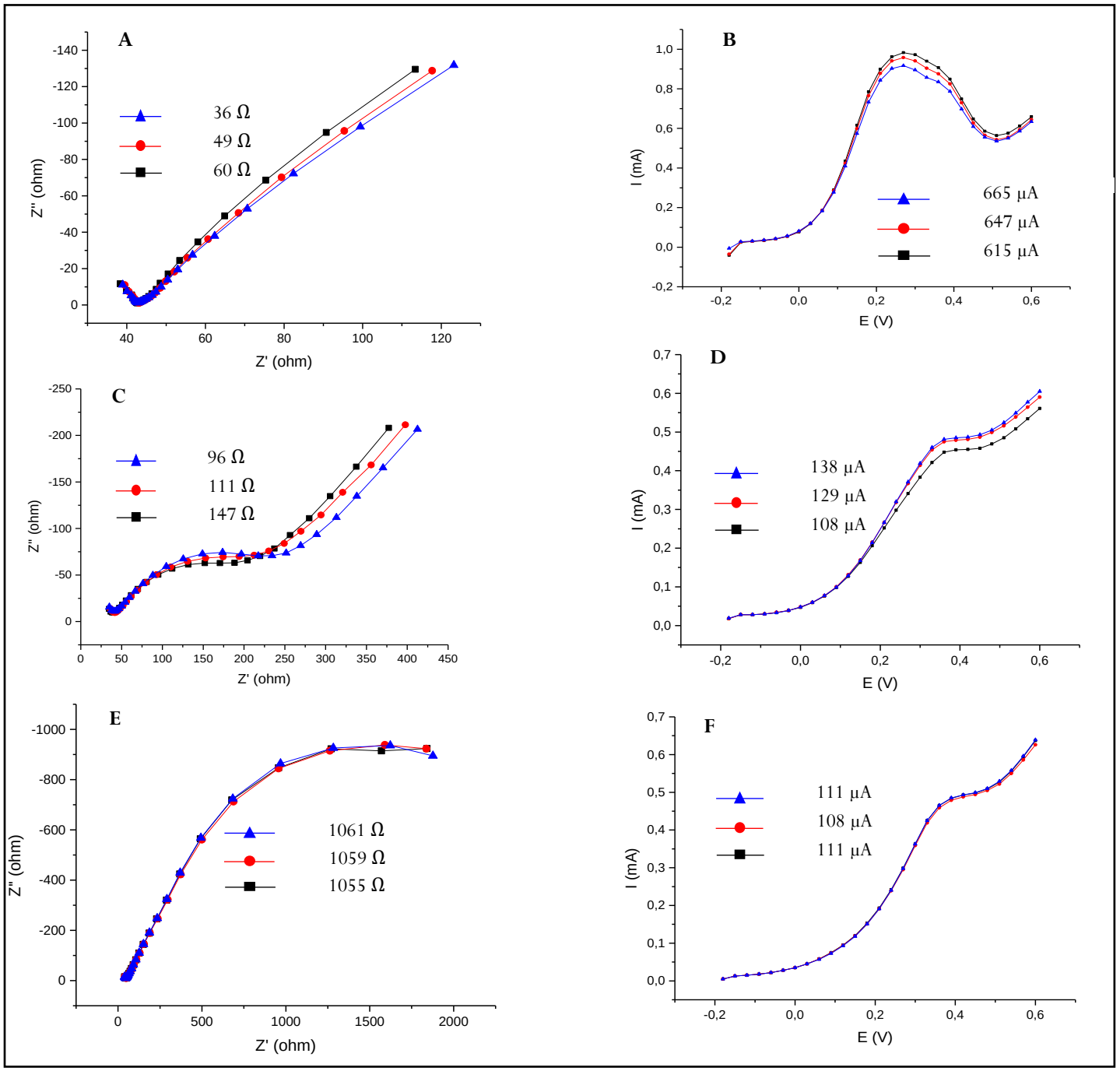

Figure S1. A) EIS and B) DPV measurements of APTES-modified pSi. C) EIS and D) DPV measurements of 4-ABA-modified pSi. E) EIS and F) DPV measurements of 4-ABH-modified pSi.